Catalysis Science & Technology

PAPER

View Article Online
View Journal | View Issue

Cite this: *Catal. Sci. Technol.*, 2015, 5, 428

A composite photocatalyst of an organic electron donor–acceptor dyad and a Pt catalyst supported on semiconductor nanosheets for efficient hydrogen evolution from oxalic acid†

Yusuke Yamada, Akifumi Nomura, Hideyuki Tadokoro and Shunichi Fukuzumi*

A composite photocatalytic system for hydrogen evolution employing acidic oxalic acid as an electron donor has been successfully constructed by combining 2-phenyl-4-(1-naphthyl)quinolinium ion ($QuPh^+$–NA), platinum (Pt) and nanosheets prepared by the exfoliation of $K_4Nb_6O_{17}$ (niobate-NS) as an organic photosensitiser, a hydrogen-evolution catalyst and a semiconductor photocatalyst for the oxidation of oxalic acid, respectively. The composite photocatalyst, $QuPh^+$–NA/niobate-NS (Pt), was prepared by a two-step route to locate a Pt catalyst near $QuPh^+$–NA on the surface of niobate-NS: (i) supporting $QuPh^+$–NA on niobate-NS by a cation exchange method and then (ii) supporting Pt on the $QuPh^+$–NA/niobate-NS by a photodeposition method using $PtCl_4^{2-}$ as a precursor, which interacts repulsively with the negatively charged surface of niobate-NS. The precursor of $PtCl_4^{2-}$ was reduced to metallic Pt by the photocatalysis of $QuPh^+$–NA in the presence of oxalate. Photocatalytic hydrogen evolution with the composite catalyst proceeds *via* photoexcitation of both niobate-NS and $QuPh^+$–NA to produce an electron and a hole in the semiconductor and the ET state ($QuPh^{\bullet}$–$NA^{\bullet+}$), respectively. The photogenerated hole of niobate-NS oxidises oxalic acid to produce CO_2 and $CO_2^{\bullet-}$ with two protons, whereas the photogenerated electron and $CO_2^{\bullet-}$ reduce $QuPh^+$–NA and the electron-transfer (ET) state to produce two equivalents of $QuPh^{\bullet}$–NA, which inject electrons to the Pt catalyst to reduce protons to hydrogen. The utilisation of oxalic acid as an electron donor even under highly acidic conditions, which are thermodynamically favourable for proton reduction to evolve hydrogen but unfavourable for oxalate oxidation, has been made possible for the first time by combining $QuPh^+$–NA, Pt and niobate-NS. Composite photocatalysts were also prepared by employing mesoporous silica-alumina and nanosheets prepared by the exfoliation of $KTiNbO_5$ (titanoniobate-NS), which possesses a band structure different from niobate-NS, as supports to clarify the requirements for a building block to achieve an active composite photocatalyst.

Received 4th August 2014,
Accepted 28th August 2014

DOI: 10.1039/c4cy01005a

www.rsc.org/catalysis

Introduction

Hydrogen (H_2) has been regarded as a potential next generation fuel because it has a high energy density per weight and there is no emission of harmful gases after use.[1] At present, H_2 supplied to industries is mainly produced by the steam reforming reaction of hydrocarbons, mostly natural gas, indicating that H_2 is not really a clean and recyclable fuel.[2] To really be a clean and recyclable fuel, H_2 should be produced from recyclable resources by utilising natural energy, such as solar energy.[3–8] In this context, photocatalytic water splitting to produce H_2 and O_2 from water by UV light irradiation has been extensively studied by using metal-oxide semiconductors such as TiO_2 supporting Pt, Ru or Ni.[9–24] The band gaps of metal-oxide semiconductors have been tuned by nitrogen or sulphur doping to improve the photoresponse to visible light for water splitting.[25,26]

In natural photosynthesis, two photosystems (I and II) are combined to achieve both the oxidation of water and the reduction of nicotinamide adenine dinucleotide (NAD^+) *via* the so called Z-scheme, to enable the utilisation of all visible light.[27] Such a Z-scheme system has been utilised to improve the photocatalysis of metal-oxide semiconductors by combining two narrow band-gap semiconductors, which are active for water oxidation and reduction under visible light irradiation, with an electron mediator, enabling the utilisation of visible

Department of Material and Life Science, Graduate School of Engineering, Osaka University, ALCA, Japan Science and Technology Agency (JST), Suita, Osaka 565-0871, Japan. E-mail: fukuzumi@chem.eng.osaka-u.ac.jp

† Electronic supplementary information (ESI) available: N_2 adsorption–desorption isotherms (Fig. S1 and S5), powder X-ray diffraction (Fig. S2, S3 and S5), TG/DTA curves (Fig. S4 and S6), IR spectra (Fig. S7), TEM images (Fig. S8), time course of absorbance change (Fig. S9), irradiance dependence of H_2 evolution rates (Fig. S10) and time course of CO_2 evolution in oxalate oxidation (Fig. S11). See DOI: 10.1039/c4cy01005a

light for water splitting.[28–32] Supporting various types of photosensitisers on semiconductors has also been widely examined to utilise visible light for water splitting.[33–40]

Compared to semiconductors, energy gaps are much easier to fine tune for organic electron donor–acceptor linked molecules, which can mimic photoinduced charge separation in the photosynthetic reaction centre.[41–44] Such photosynthetic reaction centre models with long lifetimes of charge-separated states have been utilised as photocatalysts together with water reduction catalysts for H_2 evolution, which requires relatively strong electron donors such as NADH because of the absence of efficient oxidation catalysts.[45–49] Some metal-oxide semiconductors are known to act as efficient oxidation catalysts.[9–24] Thus, the combination of photosynthetic reaction centre models and semiconductors with water reduction catalysts will enable the development of efficient photocatalytic systems for H_2 evolution, which is not possible by either of these catalytic systems alone. However, such composites of photosynthetic reaction centre models for charge separation and inorganic semiconductors have yet to be reported.

We report herein a photocatalytic H_2-evolution system using a composite photocatalyst of an organic electron donor–acceptor linked dyad, 2-phenyl-4-(1-naphthyl)quinolinium ion ($QuPh^+$–NA), which has a long electron-transfer (ET) state lifetime upon photoexcitation, and a Pt catalyst supported on semiconductor nanosheets derived from $K_4Nb_6O_{17}$ (niobate-NS) in the presence of acidic oxalic acid as an electron donor. $K_4Nb_6O_{17}$ supporting Pt or Ni has been reported to act as a photocatalyst for water splitting using a high pressure mercury lamp.[23,24] However, niobate-NS, which possesses a high surface area suitable for supporting cationic species, exhibits no such activity.[37] Oxalic acid is a naturally abundant organic compound, which has hardly been used as an electron donor for photocatalytic hydrogen evolution.[48–51] The composite catalyst has enabled to use oxalic acid as an electron donor for photocatalytic H_2 evolution by the Z-scheme system (*vide supra*), in which oxalic acid is oxidised by the holes of semiconductor nanosheets produced upon photoexcitation, whereas water is reduced by the photocatalysis of $QuPh^+$–NA with a Pt catalyst. The Pt catalyst was deposited in the close vicinity of $QuPh^+$–NA by the *in situ* reduction of anionic $PtCl_4^{2-}$, which repulsively interacts with anionic surfaces of the semiconductor nanosheets. The close location of the $QuPh^+$–NA and the Pt catalyst promotes forward electron transfer from the photoexcited $QuPh^+$–NA to the Pt catalyst. Additionally, niobate-NS of the composite catalyst was replaced with titanoniobate nanosheets prepared by the exfoliation of $KTiNbO_5$ (titanoniobate-NS) or mesoporous silica-alumina (sAlMCM-41). sAlMCM-41 is photocatalytically inactive, but is a cation exchangeable material. $K_4Nb_6O_{17}$ and $KTiNbO_5$ are semiconductors which possess cation exchangeable surfaces and strong oxidising abilities under UVA light irradiation.[22–24] Comparison of the composite catalysts in terms of photocatalysis for H_2 evolution and oxalic acid oxidation, and the lifetime of photogenerated $QuPh^{\bullet}$–$NA^{\bullet+}$ on each support, clarified the requirements to achieve an active composite catalyst for photocatalytic H_2 evolution. Although the present composite photocatalytic system is still incapable of using water as a reductant for H_2 evolution because of the absence of a water oxidation catalyst, the combination of an organic photosynthetic reaction centre model compound with semiconductor nanosheets and a water reduction catalyst, reported for the first time in this study, provides a promising perspective for further development of efficient water splitting photocatalytic systems, which may not be achieved by inorganic semiconductors alone without organic charge-separation components.

2. Result and discussion

2.1. Adsorption of $QuPh^+$–NA on metal-oxide nanosheets

Metal-oxide semiconductor nanosheets used as the oxidation catalyst of the composite catalyst were prepared by exfoliation of $K_4Nb_6O_{17}$ and $KTiNbO_5$ (niobate-NS and titanoniobate-NS) as reported in the literature,[52–54] and characterised by powder X-ray diffraction, N_2 adsorption–desorption isotherms and thermogravimetry/differential thermal analysis (TG/DTA) as shown in Fig. S1–S4 in the ESI.† The morphologies of niobate-NS and titanoniobate-NS were confirmed by TEM observations. Fig. 1a and b display TEM images of as-prepared $K_4Nb_6O_{17}$ and niobate-NS, respectively. The size of as-prepared $K_4Nb_6O_{17}$ was more than 1 μm and no mesopores were observed. On the other hand, major portions of niobate-NS formed nanoscrolls as observed in previous reports.[39] The size of the nanoscrolls was about 500–1000 nm × 10–20 nm in length and diameter as shown in Fig. 1b. A similar scroll morphology was observed for titanoniobate-NS as shown in Fig. 1c, although some particles have a sheet morphology as shown in Fig. 1d.

An organic electron donor–acceptor linked dyad of 2-phenyl-4-(1-naphthyl)quinolinium ion ($QuPh^+$–NA) was supported on niobate-NS by a cation-exchange method in a mixed solution of MeCN and water [1 : 1 (v/v)] at room temperature for 4 h. When the as-prepared $K_4Nb_6O_{17}$ was

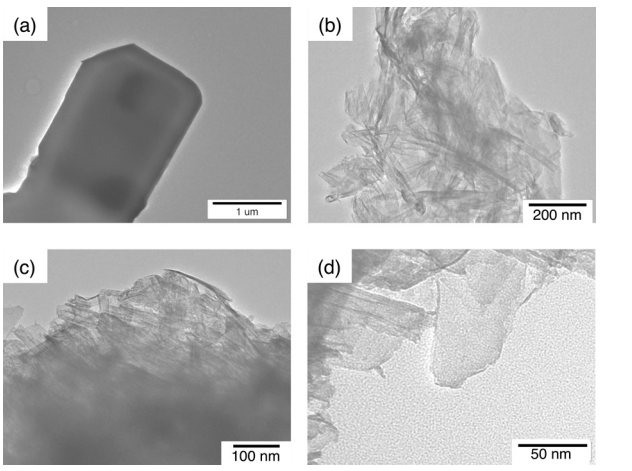

Fig. 1 TEM images of (a) as-prepared $K_4Nb_6O_{17}$, (b) exfoliated $K_4Nb_6O_{17}$ (niobate-NS) and (c, d) exfoliated $KTiNbO_5$ with scroll and sheet morphologies (titanoniobate-NS).

used as a support instead of niobate-NS, only a little amount of $QuPh^+$–NA was adsorbed because of the small Brunauer–Emmett–Teller (BET) surface area (<5 $m^2\ g^{-1}$). The loading amount of $QuPh^+$–NA on niobate-NS was determined to be 1.4×10^{-4} mol g^{-1} (4.9 wt%) by the UV-vis absorbance change of the supernatant at 334 nm, characteristic of $QuPh^+$–NA, as shown in Fig. 2a.[49,50] No significant difference was observed between niobate-NS and $QuPh^+$–NA/niobate-NS in terms of the N_2 adsorption–desorption isotherms and powder X-ray diffraction patterns (Fig. S5 in the ESI†). The amount of supported $QuPh^+$–NA estimated from the weight loss observed in TG analysis was 1.4×10^{-4} mol g^{-1} (Fig. S6a in the ESI†), which agrees with the value estimated from the UV-vis spectral change. The adsorbed $QuPh^+$–NA on the surface of niobate-NS was detected by diffuse reflectance UV-vis spectroscopy (DRS) by an increasing absorption at around 400 nm as shown in Fig. 2b. Similarly, the amount of $QuPh^+$–NA supported on titanoniobate-NS by the same method was determined to be 5.1×10^{-5} mol g^{-1} (1.8 wt%, Fig. S6b in the ESI†). The adsorption of $QuPh^+$–NA was confirmed by DRS, in which strong absorption bands appeared at wavelengths longer than 400 nm, (Fig. 2d) and IR absorption spectroscopy (Fig. S7 in the ESI†).

2.2. Preparation of photocatalysts composed of $QuPh^+$–NA/niobate-NS with negatively and positively charged Pt precursors and photocatalysis for H_2 evolution

A composite photocatalyst of $QuPh^+$–NA/niobate-NS supporting a Pt catalyst for H_2 evolution [$QuPh^+$–NA/niobate-NS (Pt)] was prepared *in situ* by photoirradiation of an aqueous suspension containing $QuPh^+$–NA/niobate-NS and K_2PtCl_4 in the presence of oxalic acid. The concentration of K_2PtCl_4 (10 μM) was much smaller than $QuPh^+$–NA (0.22 mM) based on the optimisation of the concentration of K_2PtCl_4 in the solution (Fig. 5, *vide infra*). Under photoirradiation, the photogenerated electron-transfer (ET) state of $QuPh^+$–NA ($QuPh^{\bullet}$–$NA^{\bullet+}$) reduces K_2PtCl_4 to deposit the metallic Pt catalyst on the surface of niobate-NS. Negatively charged $PtCl_4^{2-}$ was selected as a precursor to prevent the deposition of Pt^{2+} cations on niobate-NS by cation exchange. A certain amount of H_2 evolution was observed for the suspension containing $QuPh^+$–NA/niobate-NS and K_2PtCl_4 under photoirradiation (Fig. 3a, red circle). The turnover number of Pt for H_2 evolution was 250 with a turnover frequency of 21 h^{-1} for 12 h. On the other hand, no significant amount of H_2 evolution was observed when niobate-NS without $QuPh^+$–NA was used instead of $QuPh^+$–NA/niobate-NS (Fig. 3a, black square). Thus, $QuPh^+$–NA is necessary for photocatalytic H_2 evolution. Similarly, no H_2 evolution was observed by employing cationic $Pt(NH_3)_4^{2+}$ (Fig. 3a, blue triangle), which is often used to prepare platinised $K_4Nb_6O_{17}$,[24,34] as a precursor instead of K_2PtCl_4. In this case, $Pt(NH_3)_4^{2+}$ was adsorbed on the cation exchange sites of niobate-NS, to which $QuPh^+$–NA is not closely located.

For $QuPh^+$–NA/niobate-NS (Pt), CO_2 evolution accompanied by H_2 evolution with nearly two times the volume of H_2 was observed (Fig. 3b, red circle), indicating that oxalic acid acted as the electron donor. The ratio of CO_2/H_2 ranging from 1.5 to 2.0, slightly smaller than stoichiometric value (2.0), may result from a small portion of CO_2 dissolved in water. Dependence of the catalytic activity of the composite on the Pt precursors indicates that not only the preparation procedures but also the choice of a precursor is important to obtain an active composite photocatalyst for H_2 evolution.

The scroll morphology of niobate-NS was maintained after formation of $QuPh^+$–NA/niobate-NS (Pt) as confirmed by TEM observations (Fig. 4a). The Pt nanoparticles were too small to be detected by TEM for $QuPh^+$–NA/niobate-NS (Pt) after the reaction of 6 h. However, the TEM images of $QuPh^+$–NA/niobate-NS (Pt) after the reaction of 19 h show formation of Pt particles smaller than 5 nm (Fig. 4b and c). Such

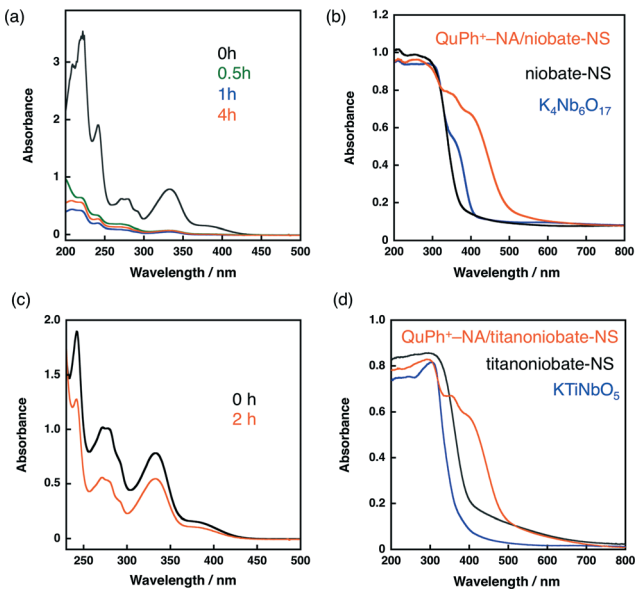

Fig. 2 (a, c) UV-vis absorption change of supernatant containing $QuPh^+$–NA by immersion of (a) niobate-NS or (c) titanoniobate-NS. (b, d) Diffuse reflectance UV-vis absorption spectra of (b) niobate-NS (black), $K_4Nb_6O_{17}$ (blue) and $QuPh^+$–NA/niobate-NS (orange) and (d) titanoniobate-NS (black), $KTiNbO_5$ (blue) and $QuPh^+$–NA/niobate-NS (orange).

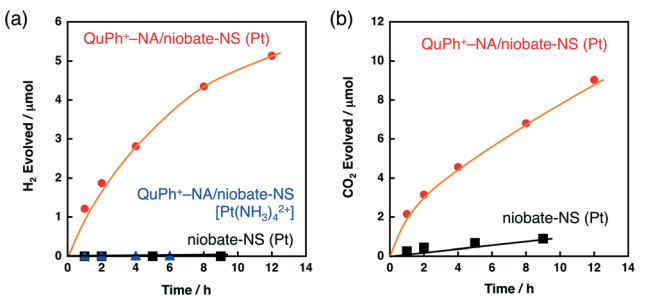

Fig. 3 Time courses of (a) H_2 and (b) CO_2 evolution during photoirradiation ($\lambda > 340$ nm) of N_2-saturated aqueous suspensions (2.0 mL, pH 1.6) containing oxalic acid (50 mM), K_2PtCl_4 (10 μM) and niobate-NS (10.0 mg) (black square); oxalic acid (50 mM), K_2PtCl_4 (10 μM) and $QuPh^+$–NA/niobate-NS (10.5 mg) (red circle); and oxalic acid (50 mM), $Pt(NH_4)_4Cl_2$ (10 μM) and $QuPh^+$–NA/niobate-NS (10.5 mg) (blue triangle).

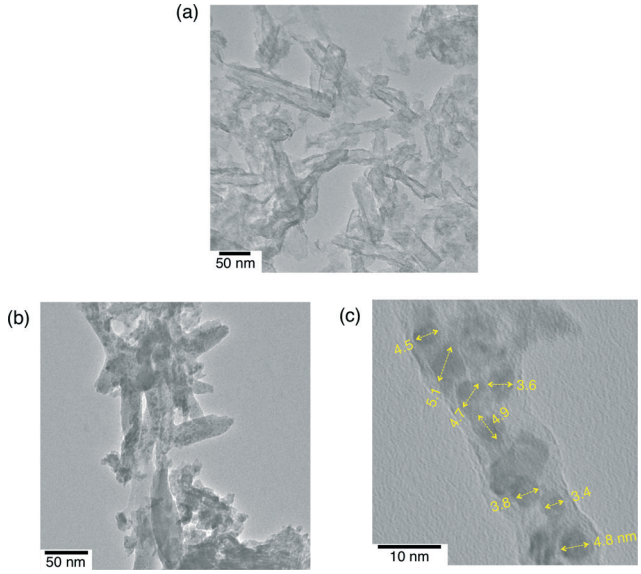

Fig. 4 TEM images of QuPh$^+$–NA/niobate-NS (Pt) after the photocatalytic reactions of (a) 6 h and (b, c) 19 h. The numbers indicate the sizes of each of the Pt nanoparticles in nm.

grown Pt particles were also observed for QuPh$^+$–NA/niobate-NS [$Pt(NH_3)_4^{2+}$] after photoirradiation (Fig. S8 in the ESI†). The highly dispersed small Pt nanoparticles exhibited high catalytic activity for H_2 evolution. The DRS of the reaction suspension indicates that nearly half of the QuPh$^+$–NA supported on niobate-NS lost its colour during the reaction of 12 h (Fig. S9 in the ESI†). Thus, the catalytic activity was lost as QuPh$^+$–NA was reduced and the size of Pt nanoparticles increased.

2.3. Optimisation of reaction conditions for photocatalytic H_2 evolution using QuPh$^+$–NA/niobate-NS (Pt)

The effect of the K_2PtCl_4 concentration on H_2 evolution was investigated for the reaction solution containing K_2PtCl_4, QuPh$^+$–NA/niobate-NS and oxalic acid. Fig. 5a shows the time courses of H_2 evolution during photoirradiation of an aqueous suspension containing oxalic acid (50 mM), QuPh$^+$–NA/niobate-NS (10.5 mg) and K_2PtCl_4 at various concentrations (2.5–40 μM) at pH 1.6. The initial H_2 evolution rate (1 h) of 0.42 μmol h^{-1} for the composite photocatalyst prepared in the presence of 2.5 μM K_2PtCl_4 was increased to 1.2 μmol h^{-1} by increasing the K_2PtCl_4 concentration to 10 μM. If all K_2PtCl_4 are reduced to metallic Pt and deposited on QuPh$^+$–NA/niobate-NS, the weight concentration of Pt is 0.37 wt% in the composite photocatalyst derived from 10 μM K_2PtCl_4. When the K_2PtCl_4 concentration was further increased to 20–40 μM, however, the amount of H_2 evolution significantly decreased (0.49 μmol with 20 μM and 0.14 μmol with 40 μM). Such a decrease in the amount of H_2 evolution may result from the increase in the size of the Pt catalyst with the larger concentration of K_2PtCl_4 (20–40 μM) during the photocatalytic reaction. Thus, the optimum K_2PtCl_4 concentration may be about 10 μM.

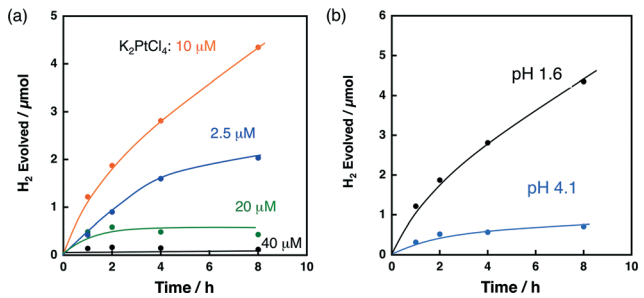

Fig. 5 (a) Time courses of H_2 evolution during photoirradiation ($\lambda > 340$ nm) of an N_2-saturated aqueous suspension (2.0 mL) containing oxalic acid (50 mM), QuPh$^+$–NA/niobate-NS (10.5 mg) and various concentrations of K_2PtCl_4 (2.5–40 μM) at pH 1.6. (b) Time courses of H_2 evolution under pH 1.6 and 4.1 conditions. The concentrations of oxalic acid, QuPh$^+$–NA/niobate-NS and K_2PtCl_4 were 50 mM, 10.5 mg and 10 μM, respectively. The pH value of each aqueous medium was controlled to 1.6 (black) or 4.1 (cyan) by adding KOH.

Then, the effect of the pH of the reaction solutions on the H_2 evolution was investigated, because the form of the oxalic acid in solution changes from the acid to the monoanion and the dianion depending on the pH of the reaction solution. The pK_{a1} and pK_{a2} values of oxalic acid (1.3 and 4.2, respectively)[55] suggest that the oxalate dianion becomes the major species in the solution of pH > 4.2. On the other hand, higher pH is thermodynamically unfavourable for proton reduction. Thus, if the oxidation of oxalic acid is a rate-determining step, the reaction rate would become maximum around pH 4.2. If the proton reduction is the rate-determining step, the reaction would become faster at a much lower pH. Fig. 5b compares the time courses of H_2 evolution from the reaction solutions containing 10 μM K_2PtCl_4 at pH 1.6 and 4.1 during photocatalytic H_2 evolution. The initial H_2 evolution rate (1 h) decreased from 1.2 μmol h^{-1} at pH 1.6 to 0.32 μmol h^{-1} at pH 4.1. Therefore, proton reduction rather than oxalate oxidation is the rate-determining step for H_2 evolution in this photocatalytic system.

The effect of irradiance was also examined by using a solar simulator (AM 1.5G). The light source contains both UVA (350 nm < λ < 400 nm) and visible light (λ > 400 nm). Photocatalytic H_2 evolution was performed by photoirradiation of an aqueous suspension (2.0 mL) in a square quartz cuvette (light path length: 10 mm) containing QuPh$^+$–NA/niobate-NS (10.5 mg), K_2PtCl_4 (10 μM) and oxalic acid (10 mM), changing the irradiance from 0.1 kW m^2 (0.1 sun) to 1 kW m^2 (1 sun). The H_2 evolution during the photocatalytic reaction was accelerated by increasing the irradiance up to 0.5 kW m^2 (0.5 sun), however, further increase of the irradiance resulted in no further increase in the H_2 evolution rate (Fig. S10 in the ESI†).

2.4. Composite photocatalysts using sAlMCM-41 and titanoniobate-NS as supports

The activity of composite photocatalysts for photocatalytic H_2 evolution is expected to depend on the supporting materials. Silica-alumina (sAlMCM-41) is a cation exchangeable but insulating material. First, photocatalytic H_2 evolution was performed under photoirradiation of a highly acidic aqueous suspension (2.0 mL, pH 0.9) containing oxalic acid (50 mM), K_2PtCl_4 (10 μM) and QuPh$^+$–NA/sAlMCM-41

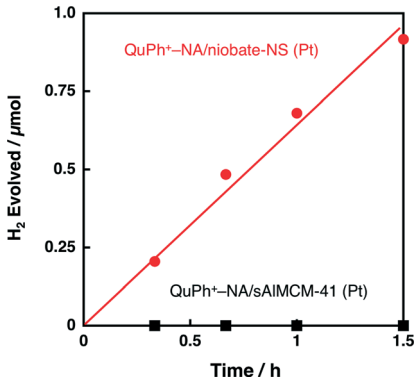

Fig. 6 Time courses of H_2 evolution during photoirradiation ($\lambda > 340$ nm) of an N_2-saturated aqueous H_2SO_4 suspension (100 mM, pH 0.9, 2.0 mL) containing oxalic acid (50 mM), K_2PtCl_4 (10 μM) and $QuPh^+$–NA supported on metal oxides [$QuPh^+$–NA/niobate-NS (10.5 mg, red circle); $QuPh^+$–NA/sAlMCM-41 (11.6 mg, black square)].

(11.6 mg, [$QuPh^+$–NA]: 0.22 mM). As indicated in Fig. 6 (black square), no H_2 evolution was observed for $QuPh^+$–NA/sAl-MCM-41 (Pt). Thus, the use of photocatalytically active niobate-NS has made it possible to evolve H_2 under these conditions by utilising its oxidising ability, which is strong enough to oxidise acidic oxalic acid.

Then, the activity of a composite photocatalyst using titanoniobate-NS instead of niobate-NS was examined, as shown in Fig. 7, where no H_2 evolution was observed under photoirradiation for 5 h (blue square), in contrast to the case of niobate-NS (red circle). The reason for the drastic difference in the photocatalytic activity between titanoniobate-NS and niobate-NS is investigated in the following sections.

2.5. Photocatalytic oxidation of oxalic acid with metal-oxide nanosheets

First, photocatalysis of niobate-NS and titanoniobate-NS for oxalic acid oxidation was confirmed by CO_2 evolution from an O_2-saturated aqueous solution (pH 1.6) containing oxalic acid, under photoirradiation ($\lambda > 340$ nm). Fig. 8 shows

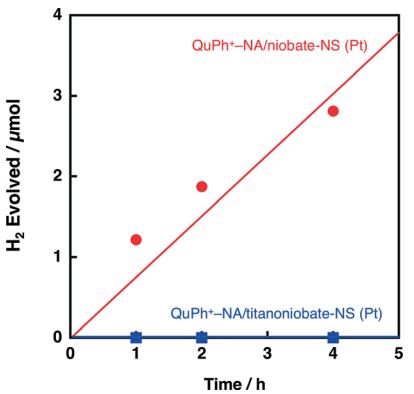

Fig. 7 Time courses of H_2 evolution during photoirradiation ($\lambda > 340$ nm) of an N_2-saturated aqueous suspension (2.0 mL, pH 1.6) containing oxalic acid (50 mM), K_2PtCl_4 (10 μM) and $QuPh^+$–NA/niobate-NS (10.5 mg, red circle) or $QuPh^+$–NA/titanoniobate-NS (10.2 mg, blue square).

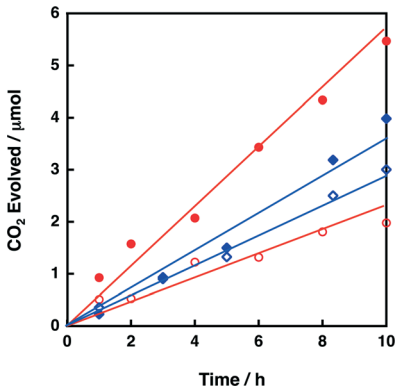

Fig. 8 Time courses of CO_2 evolution during photoirradiation ($\lambda > 340$ nm) of an O_2-saturated aqueous suspension (2.0 mL) containing oxalic acid (10 mM) and metal oxide [11.6 mg; as-prepared $K_4Nb_6O_{17}$ (red open circle), niobate-NS (red closed circle), as-prepared $KTiNbO_5$ (blue open diamond) and titanoniobate-NS (blue closed diamond)].

the time courses of CO_2 evolution during photoirradiation ($\lambda > 340$ nm) of an O_2-saturated aqueous suspension containing oxalic acid and $K_4Nb_6O_{17}$ or $KTiNbO_5$. The amount of evolved CO_2 increased linearly with the photoirradiation time for all the catalysts. The CO_2 evolution rate of 0.20 μmol h^{-1} for $K_4Nb_6O_{17}$ was increased to 0.55 μmmol h^{-1} for niobate-NS by exfoliation. The catalytic activity of niobate-NS was further enhanced by loading $QuPh^+$–NA (Fig. S11 in the ESI†). Similarly, the CO_2 evolution rate for titanoniobate-NS (0.35 μmol h^{-1}) was larger than that for $KTiNbO_5$ (0.28 μmmol h^{-1}). Thus, titanoniobate-NS can act as a photocatalyst for oxalic acid oxidation even under acidic conditions.

2.6. Photoinduced electron-transfer state of $QuPh^+$–NA ($QuPh^{\bullet}$–$NA^{\bullet+}$) on metal oxides detected by EPR spectroscopy

Photoirradiation of $QuPh^+$–NA supported on metal oxides by a 1000 W high-pressure mercury lamp through a UV-light cutting filter ($\lambda > 340$ nm) results in the formation of the triplet ET state ($QuPh^{\bullet}$–$NA^{\bullet+}$) *via* photoinduced electron transfer from the naphthalene (NA) moiety to the singlet excited state of the quinolinium ion ($QuPh^+$) moiety as evidenced by EPR measurements at −196 °C. An EPR signal at $g = 2.0031$ appearing under photoirradiation (Fig. 9a) demonstrates the formation of a radical species.[50] The weak EPR signal appearing at $g = 4.0$ demonstrates triplet multiplicity.[56] The decay rate of the EPR signal of $QuPh^{\bullet}$–$NA^{\bullet+}$ at room temperature observed after cutting off the light highly depends on the metal-oxide supports. When redox inactive sAlMCM-41 was used as a support of $QuPh^+$–NA, the decay rate in the EPR signal intensity observed after cutting off the light in Fig. 9b (i, black line) is much slower than the decay rate with metal-oxide semiconductors, niobate-NS and titanoniobate-NS (ii, red and iii, blue, respectively). The oscillation of the EPR signal intensity during intermittent photoirradiation for 2 seconds followed by approximately 50 seconds in the dark demonstrates the photorobustness of $QuPh^+$–NA on titanoniobate-NS in the presence of water (Fig. 9c).

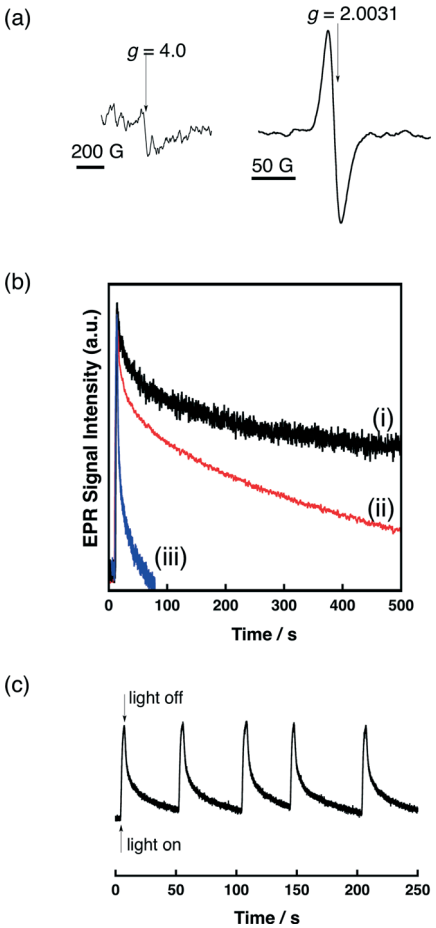

Fig. 9 (a) A typical EPR spectrum of photoinduced $QuPh^{\bullet}$–$NA^{\bullet+}$ on metal oxide ($QuPh^{+}$–NA/sAlMCM-41) using a high-pressure mercury lamp and cut off filter ($\lambda > 340$ nm). (b) Decay time profiles of the EPR signal intensity for $QuPh^{\bullet}$–$NA^{\bullet+}$ supported on (i) mesoporous silica–alumina (black), (ii) niobate-NS (red) and (iii) titanoniobate-NS (blue) at room temperature. (c) Time profiles of the EPR signal intensity for $QuPh^{\bullet}$–$NA^{\bullet+}$ supported on titanoniobate-NS in the presence of water upon intermittent photoirradiation for 2 seconds followed by approximately 50 seconds in the dark at room temperature.

The shorter lifetime of the ET state of $QuPh^{+}$–NA ($QuPh^{\bullet}$–$NA^{\bullet+}$) on the semiconductor nanosheets can be ascribed to back electron transfer facilitated by the semiconductor nanosheets, in which the $QuPh^{\bullet}$ moiety injects an electron to the semiconductor nanosheets and the injected electron reduces the $NA^{\bullet+}$ moiety. The much faster back electron transfer observed for $QuPh^{+}$–NA/titanoniobate-NS compared with that observed for $QuPh^{+}$–NA/niobate-NS can be ascribed to the difference in band structures. The band gap of $KTiNbO_5$ (3.7 V), which is wider than $K_4Nb_6O_{17}$ (3.5 V), suggests that the energy of the conduction band edge is slightly negative,[34b] because the valence band of metal-oxide semiconductors typically consists of O 2p orbitals.[57] The high reducing power of electrons in the conduction band of $KTiNbO_5$ can accelerate the back electron transfer. Another possible reason for the shorter lifetime of the ET state is the presence of adsorbed water on the surface of a metal-oxide semiconductor, because the presence of water has been reported to shorten the lifetime of $QuPh^{\bullet}$–$NA^{\bullet+}$ on sAlMCM-41 significantly.[50] However, TG/DTA analyses of $QuPh^{+}$–NA/niobate-NS and $QuPh^{+}$–NA/titanoniobate-NS suggest that weight losses due to water desorption were 8.5 and 8.7% for $QuPh^{+}$–NA/niobate-NS and $QuPh^{+}$–NA/titanoniobate-NS, respectively (Fig. S6 in the ESI†).[58] The BET surface areas of niobate-NS and titanoniobate-NS are also similar, determined to be 180 $m^2\ g^{-1}$ and 166 $m^2\ g^{-1}$, respectively. Thus, the effect of adsorbed water on the lifetime of the ET state of $QuPh^{+}$–NA on the semiconductors is negligible in this case.

2.7. Reaction mechanisms of photocatalytic H_2 evolution with $QuPh^{+}$–NA/KNb_6O_{17}-NS (Pt)

The overall photocatalytic cycle of H_2 evolution from oxalic acid with $QuPh^{+}$–NA/niobate-NS is depicted in Scheme 1. The photoirradiation of both $K_4Nb_6O_{17}$ and $QuPh^{+}$–NA resulted in the production of an electron and a hole in the semiconductor and the ET state of $QuPh^{+}$–NA, respectively. The long-lived ET state of $QuPh^{+}$–NA ($QuPh^{\bullet}$–$NA^{\bullet+}$) was reduced by the electron in the conduction band of niobate-NS and the resulting $QuPh^{\bullet}$–NA injects an electron to the Pt catalyst for H_2 evolution. The remaining hole on niobate-NS oxidises oxalic acid by electron transfer. The one-electron oxidised oxalic acid decomposes into CO_2 and $CO_2^{\bullet-}$ together with two protons. The produced $CO_2^{\bullet-}$ reduces $QuPh^{+}$–NA to produce $QuPh^{\bullet}$–NA.[48] When photoinactive and insulating sAlMCM-41 was used as a support, no oxidation of acidic oxalic acid occurred with $QuPh^{\bullet}$–$NA^{\bullet+}$, resulting in no photocatalytic H_2 evolution. In the case of titanoniobate-NS used as the support, oxalic acid oxidation proceeded by photoirradiation as shown in Fig. 8. However, the lifetime of the ET state of photogenerated $QuPh^{\bullet}$–$NA^{\bullet+}$ on titanoniobate-NS is dramatically shortened compared with that on niobate-NS (Fig. 9b), resulting in little photocatalytic activity for H_2 evolution (Fig. 7, blue square), because titanoniobate-NS may act as a better electron mediator for back electron transfer from $QuPh^{\bullet}$ to $NA^{\bullet+}$ than niobate-NS.

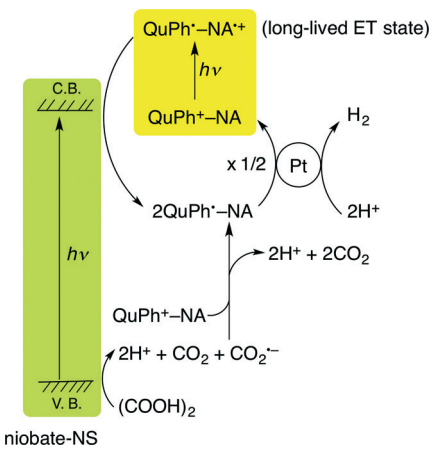

Scheme 1 The overall cycle for photocatalytic H_2 evolution with $QuPh^{+}$–NA/niobate-NS (Pt).

3. Conclusions

A composite photocatalyst for H_2 evolution was successfully prepared by rationally arranging an organic electron donor–acceptor dyad ($QuPh^+$–NA), which forms a long-lived ET state upon photoirradiation, and a Pt catalyst (proton reduction catalyst) on appropriate metal-oxide semiconductor nanosheets (niobate-NS), which act as an efficient catalyst for the photocatalytic oxidation of oxalic acid. The attractive electrostatic interaction between a Pt catalyst precursor ($PtCl_4^{2-}$) and $QuPh^+$–NA on the negatively charged surface of niobate-NS resulted in the photoreduction of $PtCl_4^{2-}$ to produce the Pt catalyst, which was closely located to $QuPh^+$–NA, for efficient H_2 evolution. When semiconductor nanosheets (niobate-NS) were replaced by similar semiconductor nanosheets (titanoniobate-NS), the photocatalytic activity for H_2 evolution was lost because of the much faster back electron transfer in the ET state of $QuPh^+$–NA *via* titanoniobate-NS. The composite photocatalyst of an organic electron donor–acceptor dyad and a Pt catalyst supported on semiconductor nanosheets for H_2 evolution developed in this study has paved a new way to combine a wide variety of organic photosynthetic reaction centre models with inorganic photocatalysts for more efficient water splitting that may not be possible by either photocatalytic component alone.

4. Experimental section

4.1. Catalyst preparation

4.1.1. Materials. All chemicals were obtained from chemical companies and used without further purification. Potassium tetrachloroplatinate(II) and niobium pentoxide were purchased from Wako Pure Chemical Industries. Tetra(*n*-butyl)ammonium hydroxide was obtained from Tokyo Chemical Industry. Potassium bicarbonate was purchased from Nacalai Tesque. 2-Phenyl-4-(1-naphthyl)quinolinium ($QuPh^+$–NA) perchlorate was synthesised by a literature method.[44] Purified water was provided by a Millipore Direct-Q3 ultrapure water system where the electronic conductance was 18.2 MΩ cm. The preparation and characterisation of $QuPh^+$–NA/mesoporous silica-alumina ($QuPh^+$–NA/sAlMCM-41) was reported elsewhere.[49,50]

4.1.2. Preparation of $K_4Nb_6O_{17}$ nanosheets (niobate-NS). Potassium niobate was prepared by a literature method.[52,53] Niobium pentoxide (8.6 g, 65 mmol) and potassium bicarbonate (3.1 g, 45 mmol) were ground together in a mortar. The obtained powder was calcined in air at 500 °C for 12 h with a ramp rate of 5 °C min^{-1}. The calcined powder was ground again and calcined at 800 °C and 1000 °C for 12 h each. The obtained powder was washed with water to remove unreacted potassium bicarbonate and dried at 85 °C. The powder X-ray diffraction of the prepared potassium niobate agreed with reported patterns. The as-prepared potassium niobate (4.0 g) was immersed in aqueous sulphuric acid (4.0 M, 100 mL) and slowly stirred to exchange potassium ions with protons for 1 day. The obtained partially proton-exchanged potassium niobate was immersed and slowly stirred in aqueous tetra(*n*-butyl)ammonium hydroxide (8.0 wt%, 200 mL) at room temperature for 1 day. The remaining precipitate was removed by centrifugation and then the supernatant was acidified with nitric acid to flocculate. The obtained precipitate was collected by centrifugation, washed with water and dried *in vacuo* overnight.

4.1.3. Preparation of potassium titanoniobate nanosheets (titanoniobate-NS). Potassium titanoniobate was prepared by a literature method.[55] Titanium dioxide (4.8 g, 60 mmol), niobium pentoxide (8.0 g, 30 mmol) and potassium bicarbonate (4.2 g, 30 mmol) were ground together in a mortar. The obtained powder was calcined at 1000 °C for 12 h with a ramp rate of 5 °C min^{-1} two times. The obtained powder was thoroughly washed with water to remove unreacted potassium bicarbonate and dried at room temperature under reduced pressure. The powder X-ray diffraction of the prepared potassium titanoniobate agreed with reported patterns. The as-prepared potassium titanoniobate (6.0 g) was immersed in aqueous hydrosulphuric acid (4.0 M, 100 mL) and slowly stirred for 1 day. The obtained partially proton exchanged potassium titanoniobate was immersed and slowly stirred in aqueous tetra(*n*-butyl)ammonium hydroxide (10 wt%, 200 mL) at room temperature for 1 day. The remaining precipitate was removed by centrifugation and then, the supernatant was acidified with nitric acid to flocculate. The obtained precipitates were collected by centrifugation, washed with water and dried *in vacuo* overnight.

4.1.4. Preparation of $QuPh^+$–NA/niobate-NS and $QuPh^+$–NA/titanoniobate-NS. $QuPh^+$–NA ion was supported on niobate-NS or titanoniobate-NS by a cation-exchange method in a mixed solution of acetonitrile and water.[49,50,56] Niobate-NS or titanoniobate-NS (100 mg) was dispersed in a mixed solution of acetonitrile and water [1 : 1 (v/v)] containing $QuPh^+$–NA (3.0 mM). The amount of exchanged $QuPh^+$–NA ion was calculated based on the decrease in absorbance at 334 nm, characteristic to the $QuPh^+$–NA ion, caused by immersion of niobate-NS or titanoniobate-NS.

4.2. Catalyst characterisation

4.2.1. Transmission Electron Microscopy (TEM). Metal-oxide semiconductors were observed from bright field images using a JEOL JEM-2100 that has a thermal field emission gun with an accelerating voltage of 200 kV. The observed samples were prepared by dropping an aqueous suspension of metal-oxide semiconductors and allowing the solvent to evaporate and then scooping up with an amorphous carbon supporting film on a meshed Cu grid.

4.2.2. Electron paramagnetic resonance (EPR). The EPR spectra were taken on a JEOL X-band spectrometer (JES-REIXE) with a quartz EPR tube (4.5 mm). The EPR spectrum of the ET state of $QuPh^+$–NA supported on a metal oxide support, which was dried under vacuum overnight, was measured under photoirradiation with a high-pressure mercury lamp (USH-1005D), through both a UV-light ($\lambda < 340$ nm) cut glass

filter and a water filter (light path length: 3 cm) to cut off IR irradiation for focusing at the sample cell in the EPR cavity, at room temperature. The *g* values were calibrated using an Mn^{2+} marker.

4.2.3. XRD, TG/DTA and DRS. Powder X-ray diffraction patterns were recorded on a Rigaku MiniFlex 600. Incident X-ray radiation was produced by a Cu X-ray tube, operating at 40 kV and 15 mA with Cu Kα radiation (λ = 1.54 Å). The scan rate was 2° min^{-1} from 2θ = 10–50°. TG/DTA measurements were performed on a SII TG/DTA 7200. A sample (about 10 mg) was loaded into an Al pan and heated under air with continuous flow. A certain amount of α-Al_2O_3 was used as a reference for DTA measurements. The sample temperature was increased at a rate of 2.5 °C min^{-1}. Nitrogen-adsorption/desorption measurements were performed at −196 °C on a Belsorp-mini (BEL Japan, Inc.) within the relative pressure range of 0.01–101.3 kPa. A sample mass of about 30 mg was used for adsorption analysis after pretreatment at 150 °C for several hours under vacuum conditions, and kept under a N_2 atmosphere for the N_2-adsorption measurements. The sample was exposed to a mixed He/N_2 gas flow with a programmed ratio, and the amount of adsorbed N_2 was calculated from the change of pressure in a cell after reaching equilibrium. Diffuse reflectance UV-vis absorption spectra were recorded by a Jasco V-670 spectrometer equipped with an SIN-768 attachment. $BaSO_4$ was used for recording background spectra.

4.3. Photocatalytic H_2 evolution

A typical experimental procedure is as follows: an aqueous suspension (2.0 mL) containing $QuPh^+$–NA/niobate-NS composite (10.5 mg, $QuPh^+$–NA: 0.74 mM), K_2PtCl_4 (10 μM) and oxalic acid (50 mM) was flushed with N_2 gas. The suspension was then photoirradiated for a certain time with a xenon lamp (Ushio Optical, Model X SX-UID 500X AMQ) through a colour filter glass (Asahi Techno Glass L39) transmitting $\lambda > 340$ nm at room temperature. After 1 min stirring in the dark, gas in a headspace was analysed by Shimadzu GC-14B gas chromatography (detector: TCD, column temperature: 50 °C, column: active carbon with a particle size 60–80 mesh, carrier gas: N_2 gas) to determine the amount of evolved H_2.

Acknowledgements

This work was supported by Grants-in-Aid (no. 24350069 and 25600025) for Scientific Research from the Japan Society for the Promotion of Science (JSPS), an ALCA project from the Japan Science and Technology Agency (JST), and NRF of Korea through the GRL (2010-00353) program. We sincerely acknowledge the Research Centre for Ultra-Precision Science & Technology, Osaka University for TEM measurements.

Notes and references

1 (*a*) S. Dunn, in *Encyclopedia of Energy*, Elsevier Inc., 2004, vol. 3, pp. 241–252; (*b*) M. Momirlan and T. N. Veziroglub, *Int. J. Hydrogen Energy*, 2005, **30**, 795–802; (*c*) National research council and national academy of engineering of the national academies, *The Hydrogen Economy: Opportunities, Costs, Barriers, and R&D Needs*, The National Academies Press, Washington, D.C., 2004.

2 G. Laurenczy, in *Encyclopedia of Catalysis*, ed. I. T. Horvath, Wiley-Interscience, Hoboken, NJ, 2010.

3 (*a*) H. B. Gray, *Nat. Chem.*, 2009, **1**, 7–7; (*b*) N. S. Lewis and D. G. Nocera, *Proc. Natl. Acad. Sci. U. S. A.*, 2006, **103**, 15729–15735; (*c*) D. G. Nocera, *Chem. Soc. Rev.*, 2009, **38**, 13–15; (*d*) T. A. Faunce, W. Lubitz, A. W. B. Rutherford, D. MacFarlane, G. F. Moore, P. Yang, D. G. Nocera, T. A. Moore, D. H. Gregory, S. Fukuzumi, K. B. Yoon, F. A. Armstrong, M. R. Wasielewski and S. Styring, *Energy Environ. Sci.*, 2013, **6**, 695–698.

4 (*a*) Y. Amao, *ChemCatChem*, 2011, **3**, 458–474; (*b*) P. D. Tran, L. H. Wong, J. Barber and J. S. C. Loo, *Energy Environ. Sci.*, 2012, **5**, 5902–5918; (*c*) S. Bensaid, G. Centi, E. Garrone, S. Perathoner and G. Saracco, *ChemSusChem*, 2012, **5**, 500–521.

5 (*a*) D. G. Nocera, *Acc. Chem. Res.*, 2012, **45**, 767–776; (*b*) M. Wang, L. Chen and L. Sun, *Energy Environ. Sci.*, 2012, **5**, 6763–6778; (*c*) S. Y. Reece, J. A. Hamel, K. Sung, T. D. Jarvi, A. J. Esswein, J. J. H. Pijpers and D. G. Nocera, *Science*, 2011, **334**, 645–648.

6 (*a*) R. M. Bullock, A. M. Appel and M. L. Helm, *Chem. Commun.*, 2014, **50**, 3125–3143; (*b*) P. V. Kamat, *J. Phys. Chem. C*, 2007, **111**, 2834–2860; (*c*) A. J. Bard and M. A. Fox, *Acc. Chem. Res.*, 1995, **28**, 141–145; (*d*) Y. Qu and X. Du, *Chem. Soc. Rev.*, 2013, **42**, 2568–2580.

7 (*a*) Y. Halpin, M. T. Pryce, S. Rau, D. Dinic and J. G. Vos, *Dalton Trans.*, 2013, **42**, 16243–16254; (*b*) P. D. Frischmann, K. Mahata and F. Wüthner, *Chem. Soc. Rev.*, 2013, **42**, 1847–1870; (*c*) B. van den Bosch, H.-C. Chen, J. I. van der Vlugt, A. M. Brouwer and J. N. H. Reek, *ChemSusChem*, 2013, **6**, 790–793.

8 (*a*) S. Fukuzumi, *Eur. J. Inorg. Chem.*, 2008, 1351–1362; (*b*) V. S. Thoi, Y. Sun, J. R. Long and C. J. Chang, *Chem. Soc. Rev.*, 2013, **42**, 2388–2400; (*c*) S. Fukuzumi, Y. Yamada, T. Suenobu, K. Ohkubo and H. Kotani, *Energy Environ. Sci.*, 2011, **4**, 2754–2766.

9 (*a*) A. Fujishima and K. Honda, *Nature*, 1972, **238**, 37; (*b*) A. Fujishima, X. Zhang and D. A. Tryk, *Int. J. Hydrogen Energy*, 2007, **32**, 2664.

10 (*a*) A. Kudo and Y. Miseki, *Chem. Soc. Rev.*, 2009, **38**, 253–278; (*b*) A. Kudo, *Int. J. Hydrogen Energy*, 2007, **32**, 2673.

11 (*a*) K. Takanabe and K. Domen, *ChemCatChem*, 2012, **4**, 1485–1497; (*b*) K. Maeda and K. Domen, *J. Phys. Chem. Lett.*, 2010, **1**, 2655–2661.

12 F. E. Osterloh, *Chem. Mater.*, 2008, **20**, 35–54.

13 X. Chen, S. Shen, L. Guo and S. S. Mao, *Chem. Rev.*, 2010, **110**, 6503–6570.

14 J. S. Lee, *Catal. Surv. Asia*, 2006, **9**, 217–227.

15 M. G. Walter, E. L. Warren, J. R. McKone, S. W. Boettcher, Q. Mi, E. A. Santori and N. S. Lewis, *Chem. Rev.*, 2010, **110**, 6446–6473.

16 H. Zhou, T. Fan and D. Zhang, *ChemSusChem*, 2011, **3**, 513–528.

17 J. Yang, D. Wang, H. Han and A. C. Li, *Acc. Chem. Res.*, 2013, **46**, 1900–1909.
18 P. F. Ji, M. Takeuchi, T. M. Cuong, J. L. Zhang, M. Matsuoka and M. Anpo, *Res. Chem. Intermed.*, 2010, **36**, 327–347.
19 R. M. Navarro, M. C. Alvarez-Galvan, J. A. V. de la Mano, S. M. Al-Zahrani and J. L. G. Fierro, *Energy Environ. Sci.*, 2010, **3**, 1865–1882.
20 R. M. N. Yerga, M. C. A. Galvan, F. del Valle, J. A. V. de la Mano and J. L. Fierro, *ChemSusChem*, 2009, **2**, 471–485.
21 H. Kato, K. Asakura and A. Kudo, *J. Am. Chem. Soc.*, 2003, **125**, 3082–3089.
22 (*a*) K. Domen, A. Kudo, A. Shinozaki, A. Tanaka, K. Maruya and T. Onishi, *J. Chem. Soc., Chem. Commun.*, 1986, 356–357; (*b*) K. Domen, A. Kudo, M. Shibata, A. Tanaka, K. Maruya and T. Onishi, *J. Chem. Soc., Chem. Commun.*, 1986, 1706–1707.
23 (*a*) A. Kudo, A. Tanaka, K. Domen, K. Maruya, K. Aika and T. Onishi, *J. Catal.*, 1988, **111**, 67–76; (*b*) A. Kudo, K. Sayama, A. Tanaka, K. Asakura, K. Domen, K. Maruya and T. Onishi, *J. Catal.*, 1989, **120**, 337–352.
24 (*a*) K. Sayama, A. Tanaka, K. Domen, K. Maruya and T. Onishi, *Catal. Lett.*, 1990, **4**, 217–222; (*b*) K. Sayama, A. Tanaka, K. Domen, K. Maruya and T. Onishi, *J. Phys. Chem.*, 1991, **95**, 1345–1348; (*c*) K. Sayama, K. Yase, H. Arakawa, K. Asakura, A. Tanaka, K. Domen and T. Onishi, *J. Photochem. Photobiol., A*, 1998, **114**, 125–135.
25 (*a*) J. Hou, Z. Wang, W. Kan, S. Jiao, H. Zhu and R. V. Kumar, *J. Mater. Chem.*, 2012, **22**, 7291–7299; (*b*) J. E. Yourey, J. B. Kurtz and B. M. Bartlett, *J. Phys. Chem. C*, 2012, **116**, 3200–3206; (*c*) P. Lei, F. Wang, S. Zhang, Y. Ding, J. Zhao and M. Yang, *ACS Appl. Mater. Interfaces*, 2014, **6**, 2370–2376.
26 (*a*) Y. Moriya, T. Takata and K. Domen, *Coord. Chem. Rev.*, 2013, **257**, 1957–1969; (*b*) K. Maeda, D. Lu and K. Domen, *Chem. – Eur. J.*, 2013, **19**, 4986–4991; (*c*) M. Higashi, K. Domen and R. Abe, *J. Am. Chem. Soc.*, 2012, **134**, 6968–6971; (*d*) K. Maeda and K. Domen, *J. Phys. Chem. C*, 2007, **111**, 7851–7861; (*e*) K. Maeda, K. Teramura and K. Domen, *J. Catal.*, 2008, **254**, 198–204.
27 A. J. Bard, *J. Photochem.*, 1979, **10**, 59–75.
28 (*a*) R. Abe, K. Shinmei, N. Koumura, K. Hara and B. Ohtani, *J. Am. Chem. Soc.*, 2013, **135**, 16872–16884; (*b*) R. Abe, K. Sayama, K. Domen and H. Arakawa, *Chem. Phys. Lett.*, 2001, **344**, 339–344; (*c*) R. Abe, *J. Photochem. Photobiol., C*, 2011, **11**, 179–209.
29 W. Fan, Q. Zhang and Y. Wang, *Phys. Chem. Chem. Phys.*, 2013, **15**, 2632–2649.
30 K. Sayama, K. Mukasa, R. Abe, Y. Abe and H. Arakawa, *Chem. Commun.*, 2001, 2416–2417.
31 (*a*) A. Kudo, *MRS Bull.*, 2011, **36**, 32–38; (*b*) Q. Jia, A. Iwase and A. Kudo, *Chem. Sci.*, 2014, **5**, 1513–1519; (*c*) Y. Sasaki, A. Iwase, H. Kato and A. Kudo, *J. Catal.*, 2008, **259**, 133–137; (*d*) Y. Sasaki, H. Kato and A. Kudo, *J. Am. Chem. Soc.*, 2013, **135**, 5441–5449.
32 (*a*) K. Maeda, M. Higashi, D. Lu, R. Abe and K. Domen, *J. Am. Chem. Soc.*, 2010, **132**, 5858–5868; (*b*) K. Maeda, R. Abe and K. Domen, *J. Phys. Chem. C*, 2011, **115**, 3057–3064; (*c*) K. Maeda, *ACS Catal.*, 2013, **3**, 1486–1503.
33 H. Gerischer, *Photochem. Photobiol.*, 1972, **16**, 243–260.
34 (*a*) Y. I. Kim, S. Salim, M. J. Huq and T. E. Mallouk, *J. Am. Chem. Soc.*, 1991, **113**, 9561–9563; (*b*) Y. I. Kim, S. J. Atherton, E. S. Brigham and T. E. Mallouk, *J. Phys. Chem.*, 1993, **97**, 11802–11810; (*c*) W. J. Youngblood, S.-H. A. Lee, K. Maeda and T. E. Mallouk, *Acc. Chem. Res.*, 2009, **42**, 1966–1973.
35 T. Nakato, K. Kuroda and C. Kato, *Chem. Mater.*, 1992, **4**, 128–132.
36 K. Mori, S. Ogawa, M. Martis and H. Yamashita, *J. Phys. Chem. C*, 2012, **116**, 18873–18877.
37 T. K. Townsend, E. M. Sabio, N. D. Browning and F. E. Osterloh, *ChemSusChem*, 2011, **4**, 185–190.
38 S. Uchida, Y. Yamamoto, Y. Fujishiro, A. Watanabe, O. Ito and T. Sato, *J. Chem. Soc., Faraday Trans.*, 1997, **93**, 3229–3234.
39 K. Maeda, M. Eguchi, W. J. Youngblood and T. E. Mallouk, *Chem. Mater.*, 2008, **20**, 6770–6778.
40 (*a*) H. Hagiwara, T. Inoue, K. Kaneko and T. Ishihara, *Chem. – Eur. J.*, 2009, **15**, 12862–12870; (*b*) H. Hagiwara, M. Nagatomo, C. Seto, S. Ida and T. Ishihara, *J. Photochem. Photobiol., A*, 2013, **272**, 41–48; (*c*) H. Hagiwara, T. Inoue, S. Ida and T. Ishihara, *Phys. Chem. Chem. Phys.*, 2011, **13**, 18031–18037.
41 (*a*) M. R. Wasielewski, *Acc. Chem. Res.*, 2009, **42**, 1910–1921; (*b*) D. Gust, T. A. Moore and A. L. Moore, *Acc. Chem. Res.*, 2009, **42**, 1890–1898; (*c*) D. Gust, T. A. Moore and A. L. Moore, *Acc. Chem. Res.*, 1993, **26**, 198–205.
42 (*a*) S. Fukuzumi, K. Ohkubo and T. Suenobu, *Acc. Chem. Res.*, 2014, **47**, 1455–1464; (*b*) S. Fukuzumi, *Phys. Chem. Chem. Phys.*, 2008, **10**, 2283–2297; (*c*) S. Fukuzumi and K. Ohkubo, *J. Mater. Chem.*, 2012, **22**, 4575–4587; (*d*) S. Fukuzumi, *Org. Biomol. Chem.*, 2003, **1**, 609–620.
43 S. Fukuzumi, H. Kotani, K. Ohkubo, S. Ogo, N. V. Tkachenko and H. Lemmetyinen, *J. Am. Chem. Soc.*, 2004, **126**, 1600–1601.
44 H. Kotani, K. Ohkubo and S. Fukuzumi, *Faraday Discuss.*, 2012, **155**, 89–102.
45 (*a*) H. Kotani, K. Ohkubo, Y. Takai and S. Fukuzumi, *J. Phys. Chem. B*, 2006, **110**, 24047–24053; (*b*) H. Kotani, T. Ono, K. Ohkubo and S. Fukuzumi, *Phys. Chem. Chem. Phys.*, 2007, **9**, 1487–1492; (*c*) H. Kotani, R. Hanazaki, K. Ohkubo, Y. Yamada and S. Fukuzumi, *Chem. – Eur. J.*, 2011, **17**, 2777–2785.
46 (*a*) Y. Yamada, T. Miyahigashi, H. Kotani, K. Ohkubo and S. Fukuzumi, *J. Am. Chem. Soc.*, 2011, **133**, 16136–16145; (*b*) Y. Yamada, S. Shikano and S. Fukuzumi, *J. Phys. Chem. C*, 2013, **117**, 13143–13152.
47 Y. Yamada, T. Miyahigashi, H. Kotani, K. Ohkubo and S. Fukuzumi, *Energy Environ. Sci.*, 2012, **5**, 6111–6118.
48 Y. Yamada, T. Miyahigashi, K. Ohkubo and S. Fukuzumi, *Phys. Chem. Chem. Phys.*, 2012, **14**, 10564–10571.
49 Y. Yamada, H. Tadokoro and S. Fukuzumi, *RSC Adv.*, 2013, **3**, 25677–25680.
50 Y. Yamada, A. Nomura, K. Ohkubo, T. Suenobu and S. Fukuzumi, *Chem. Commun.*, 2013, **49**, 5132–5134.

51 (*a*) D. B. Haytowitz and R. H. Matthews, *Agriculture Handbook No. 8–11, Science and Education Administration*, USDA, Washington, D.C., 1984; (*b*) E. A. Malinka and G. L. Kamalov, *React. Kinet. Catal. Lett.*, 1993, **52**, 13–18; (*c*) E. A. Malinka and G. L. Kamalov, *J. Photochem. Photobiol., A*, 1994, **81**, 193–197; (*d*) E. A. Malinka, G. L. Kamalov, S. V. Vodzinskii, V. I. Melnik and Z. I. Zhilina, *J. Photochem. Photobiol., A*, 1995, **90**, 153–158.
52 K. Nassau, J. W. Shiever and J. L. Bernstein, *J. Electrochem. Soc.*, 1969, **116**, 348–353.
53 A. D. Wadsley, *Acta Crystallogr.*, 1964, **17**, 623–628.
54 G. H. Du, Y. Yu, Q. Chen, R. H. Wang, W. Zhou and L. M. Peng, *Chem. Phys. Lett.*, 2003, **377**, 445–448.
55 R. C. Weast, in *Handbook of Chemistry and Physics*, CRC, Cleaveland, OH, 56th edn, 1975–1976.
56 S. Fukuzumi, K. Doi, A. Itoh, T. Suenobu, K. Ohkubo, Y. Yamada and K. D. Karlin, *Proc. Natl. Acad. Sci. U. S. A.*, 2012, **109**, 15572–15577.
57 D. E. Scaife, *Sol. Energy*, 1980, **25**, 41–54.
58 M. A. Bizeto and V. R. L. Constantino, *Mater. Res. Bull.*, 2004, **39**, 1729–1736.